## Title
Physicochemical and biochemical spatiotemporal maps of a mouse penis



## Authors
Hennefarth, Matthew R
Chen, Ling
Wang, Bohan
et al.

## Publication Date
2020-03-01

## DOI
10.1016/j.jbiomech.2020.109637

Peer reviewed

Journal of Biomechanics 101 (2020) 109637

Contents lists available at ScienceDirect

Journal of Biomechanics

journal homepage: www.elsevier.com/locate/jbiomech
www.JBiomech.com

# Physicochemical and biochemical spatiotemporal maps of a mouse penis

Matthew R. Hennefarth [a], Ling Chen [a], Bohan Wang [b], Tom F. Lue [b], Marshall L. Stoller [b], Guiting Lin [b], Misun Kang [a], Sunita P. Ho [a,b,*,1]

[a] Division of Biomaterials and Bioengineering, Department of Preventive and Restorative Dental Sciences, School of Dentistry, University of California San Francisco, San Francisco, CA, United States
[b] Department of Urology, School of Medicine, University of California San Francisco, San Francisco, CA, United States

ARTICLE INFO

*Article history:*
Accepted 13 January 2020

*Keywords:*
Biomechanics
Baculum
Mouse penis
Elastin
Collagen
Mechanobiology

ABSTRACT

Spatiotemporal mechanobiology resulting in penile pathologies continues to be investigated using small scale animals models such as mice. However, species-dependent functional biomechanics of a mouse penis, is not known. In this study, spatial mapping of a mechanosensitive transcription factor, scleraxis (Scx), at ages 4, 5, 6 weeks, and 1 year were generated to identify mechanoactive regions within penile tissues. Reconstructed volumes of baculum collected using micro X-ray computed tomography illustrated significantly increased baculum length with decreased porosity, and increased mineral density ($p < 0.05$) with age. The bony-baculum was held centrally in the Scx positive corpus cavernosum glandis (CCG), indicating mechanoactivity within the struts in a 6 week old mouse. The struts also were stained positive for fibrillar proteins including collagen and elastin, and globular proteins including protein gene product 9.5, and α-smooth muscle actin. The corpus cavernosum penis (CCP) contained significantly ($p < 0.05$) more collagen than CCG within the same penis, and both regions contained blood vessels with equivalent innervation at any given age. Comparison of volumes of flaccid and erect penile forms revealed functional characteristics of the CCP. Results of this study provided insights into biomechanical function of the CCG; in that, it is a high-pressure chamber that stiffens the penis and is similar to the human corpus cavernosum.



## 1. Introduction

In most mammals, the baculum, also known as the os penis, is a bony structure that is situated within the glans or septum of the penis (Burt, 1936; Gilbert and Zevit, 2001; Yilmaz et al., 2013). Unlike humans, most non-human primates have a baculum that varies in size and composition (Ankel-Simons, 2007; Brindle and Opie, 2016; Schultz et al., 2016). However, the function and morphology of the baculum, in general, tends to vary between species (Herdina et al., 2010; Sharir et al., 2011; Stockley et al., 2013).

From a biomechanics perspective, the mineralized baculum is hypothesized to predominantly bear loads during copulation, presumably during function, in comparison to the dynamic load bearing bone of the musculoskeletal system or the alveolar bone of the dental, oral, and craniofacial masticatory system (DOC-MS). Congruent with passive load-mediated adaptation that occurs during development and active load-mediated functional adaptation that occurs during function mediated growth, at any given age, the mineral density of a canine baculum is noticeably lower when compared to its dynamically load-bearing radii (Sharir et al., 2011).

Stiffening of the corpus cavernosum of a mouse penis (CCP) resulting from nerve stimulation and engorgement during function allows us to ask: what are the forces that act on the baculum per se, and what are the forces that the baculum would exert on the adjacent tissues? The rat baculum, in general, is thought to act as a piston. As an external force is applied, the baculum is pushed into the CCP. The internal volume of the CCP decreases, and the intracavernosal pressure and rigidity of the CCP increases enabling intended organ function (Kelly, 2000). Rodents, additionally possess an ischiocavernosus muscle, which has been shown to contract and increase the pressure by several hundred millimeters of mercury within the CCP even after it is filled with blood (Beckett et al., 1974, 1972; Dean and Lue, 2005; Hanyu et al., 1987; Phillips et al., 2015). This additional pressure is thought to augment functional forces by permitting a rigid CCP and an erection that would facilitate copulation. Despite this noticeable biomechanical function, no studies to date have reported on anatomy-

* Corresponding author at: 707 Parnassus Avenue, D 3212, School of Dentistry, University of California San Francisco, San Francisco, CA 94143, United States.
*E-mail address:* sunita.ho@ucsf.edu (S.P. Ho).
[1] Lab address: Health Sciences West (HSW) 813, 513 Parnassus Avenue, University of California San Francisco, San Francisco, CA 94143, United States.

https://doi.org/10.1016/j.jbiomech.2020.109637
0021-9290/

specific mechanoactive sites within softer tissues and their intimate interfaces with the bony-baculum. Furthermore, the mouse penis is often used as model for studying diseases such as Peyronie's disease (PD) (Bivalacqua et al., 2000; Davila et al., 2003; El-Sakka et al., 1997) and erectile dysfunction (ED) (Kifor et al., 1997; Martínez-Piñeiro et al., 1994; Penson et al., 1997; Piao et al., 2007). There are several rodent models for studying Peyronie's plaque formation including TGF β1 injection (El-Sakka et al., 1997), fibrin (Davila et al., 2003), surgical (Ferretti et al., 2014), and genetic models (Lucattelli et al., 2008) where the target tissue is the tunica albuginea of the CCP, which is analogous to the human corpus cavernosum (CC).

In this study scleraxis-green fluorescence protein (Scx-GFP) transgenic mice were used. It is hypothesized that the scleraxis (Scx) transcription factor localizes within biomechanically active tissues that experience shifts in mechanical strain similar to ligaments and tendons of the musculoskeletal system (Schweitzer et al., 2001) and the DOC-MS (Lee et al., 2015; Scott et al., 2011). The specific objectives in this study are (1) to map Scx localization within a mouse penis in relation to the baculum and investigate its age-related expression level changes in the mechanoactive/responsive tissues, and (2) to colocalize nerves, smooth muscle cells (SMC), collagen, and elastin (key proteins and cells involved in penile biomechanics) within different tissues of a mouse penis.

## 2. Materials and methods

### 2.1. Micro X-ray computed tomography to map the form of an erect penis, and structure and mineral density of baculum

A total of fourteen non-sexually active Scx-GFP mice (N = 14) were used (Lee et al., 2015; Pryce et al., 2007; Scott et al., 2011; Sugimoto et al., 2013). Twelve Scx-GFP mice of ages 4 weeks, 5 weeks, 6 weeks, and 1 year with three mice per age group (n = 3) were used for mineral density and histological analyses. Two Scx-GFP mice of ages 6 and 9 weeks were used for gross/macroscale visualization of soft and hard tissue structures using a micro X-ray computed tomography (micro-XCT) (MicroXCT-200; Carl Zeiss Microscopy, Pleasanton, CA). General quantitative morphological differences during flaccid and erect states of penis were analyzed using AVIZO post-analysis software (Version 9.3.0; FEI, Hillsboro, Oregon). All experiments were conducted within the guidelines of the Institutional Animal Care and Use Committee of UCSF, protocol AN148450. Mice were euthanized and the penis was dissected, fixed overnight in 10% neutral buffered formalin (NBF) at 4 °C, washed in 1X phosphate-buffered saline (PBS) twice, and stored in a 50% ethanol/water solution at 4 °C.

Erection of a mouse penis *ex vivo* and subsequent imaging of it using a micro-XCT was performed by injecting 10% NBF into the CCP of an anesthetized 6 and 9 week old mice (Fig. S1). The penis was harvested by separating it from the body using a string. These penile specimens were soaked in 2% w/v iodine in ethanol overnight followed by 1% w/v phosphotungstic acid (70% ethanol, pH = 2.71) overnight to enhance X-ray contrast (Nieminen et al., 2015). The tissues were washed twice in 50% ethanol and were scanned using a micro-XCT at a power of 40 W. 1200 image projections were collected at 4X magnification (4.5 μm/voxel) and were analyzed using AVIZO. An average mineral density gradient was evaluated by calculating the mineral density over each virtual section along the normalized length of the mineralized baculum as previously described (Djomehri et al., 2015). For structural analysis of the baculum, an intensity threshold was applied to digitally segment the mineralized baculum and the pores from the surrounding radiopaque and radiotransparent regions.

### 2.2. Histology and immunohistochemistry of various compartments and tissue structures within a mouse penis

Following scanning with a micro-XCT, tissues were decalcified in 0.5 M EDTA (pH = 8.0) at 4 °C and were chemically processed and embeddeded in paraffin from which 6 μm thick sagittal sections (Fig. S2) were cut from using a microtome. Sections were deparaffinized and stained using Gills's hematoxylin number 2 (Hematoxylin Solution, Gill No. 2; GHS216-500ML; Sigma-Aldrich, St. Louis, MO) and counterstained with eosin Y (H&E) (Eosin Y Stain; STE0143; American MasterTech, Lodi, CA) to determine relative localization of cells and matrix proteins, and Massons' trichrome (Masson's Trichrome Stain Kit; 25088-1; Polysciences Inc, Warrington, PA) for collagen distribution, and Verhoeff's stain (Verhoeff Elastin Stain Kit; KTVEL; American MasterTech, Lodi, CA) was used for elastin localization.

For immunolocalization of various proteins using DAB and fluorescent probes, sections were blocked with 5% normal goat serum (S-1000; Vector Labs, Burlingame, CA) in 2.5% bovine serum albumin (9048-46-8; Millipore Sigma, St. Louis, MO) for 1 h, then incubated with either the primary rabbit anti-α smooth muscle actin (α-SMA) antibody (1:200; ab5694; Abcam, Cambridge, MA) or anti-protein gene product 9.5 (PGP) antibody (1:200; ab108986; Abcam) overnight at 4 °C. Sections immunolocalized for the PGP antigen were stained with a secondary antibody kit (Vectastain Elite ABC HRP Kit, PK-6101, Vector Laboratories, Inc.) and DAB substrate kit (ImmPACT DAB peroxidase (HRP) substrate; SK-4105; Vector Laboratories, Inc.) prior to staining with modified Mayers hematoxylin (HXMMHPT; American MasterTech, Lodi, CA). Sections immunolocalized for the α–SMA antigen were incubated with a secondary fluorescent antibody Goat Anti-Rabbit IgG H&L (Alexa Fluor 555) (1:200; ab150078; Abcam) for 90 min and cell nuclei were counterstained using Hoeschst 3342 (DAPI) (0.1 μg/mL; H3570; Molecular Probes, Eugene, OR) for 1 min (see Fig. S3 for blank control). Histomorphometric analysis was performed on light micrographs collected from serial sections using a light microscope (Zeiss Axio Observer.Z1; Carl Zeiss Microscopy). All sections were viewed on an inverted microscope and images were captured with Zen (Version 2.3; Carl Zeiss Microscopy) data acquisition software. Fluorescent images were captured with a 1 s exposure. Images were exported to ImageJ Fiji Edition Version 2.0 (continuous release version; NIH, Bethseda, MD) to subtract background fluorescence. The resulting images were overlaid with brightfield images to illustrate co-localization of proteins within tissue structure. The same sections were additionally viewed under a field emission – scanning electron microscope (SIGMA 500-VP Field Emission Electron Microscope – Scanning and Transmission; Carl Zeiss Microscopy) at 1 keV in order to detect erythrocytes within the corpus cavernosum glandis (CCG) and CCP.

Elastic orientation was identified by rotating the images until the baculum was parallel to the horizontal axis. The region of interest (ROI) within the CCG was selected to evaluate elastin orientation using OrientationJ plug-in (Fonck et al., 2009; Püspöki et al., 2016). The density of elastin, collagen, and smooth muscle cells were determined for the 12 Scx-GFP mice (3 mice per age group, and 4 ages) by using 4 slides per mouse with 4 sections per slide, totaling 16 sections per age. Statistical analysis was performed to highlight significant differences in elastin orientation with age.

### 2.3. Statistical analysis

Results were expressed as mean ± standard error of the mean (SEM). Pearson's correlation tests were used to determine if significant correlation existed between two variables using a variety of statistical and graphical packages within R (Auguie, 2016; Harrel and Dupont, 2017; R Core Team, 2017; Wickham, 2016). Welch's

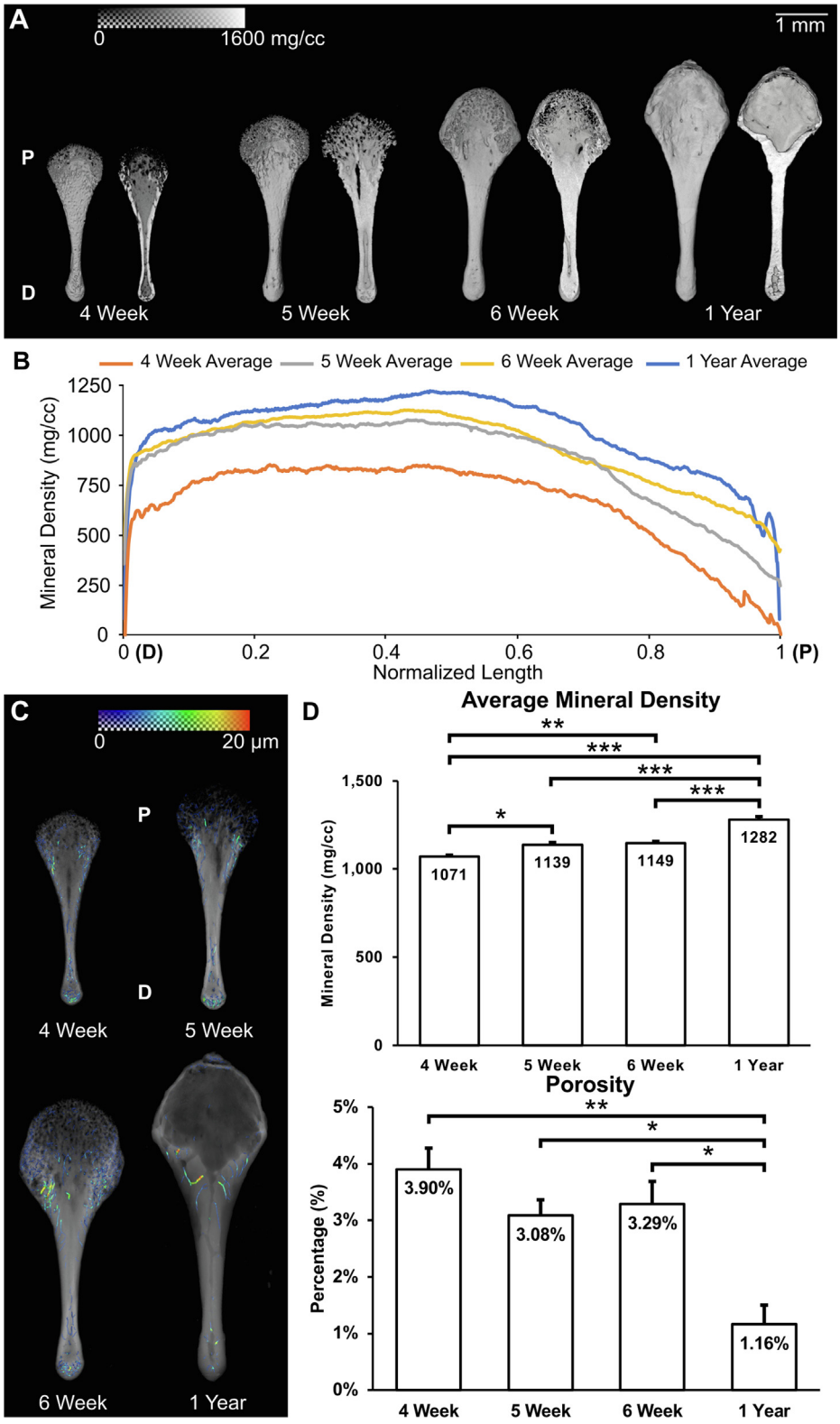


**Fig. 1.** Mineral density and porosity illustrate continuous growth of baculum at the proximal end past sexual maturity. **(A)** 3D reconstruction of the baculum (left) at each age group accompanied with 3D coronal sections of the baculum illustrate the internal structure (right). Images on the right show the medullary canal and porous nature of the bone specifically at the proximal end of the baculum. Mineral density is represented in grayscale from 0 to 1600 mg/cc. **(B)** Average mineral density gradients from distal to proximal ends along the normalized length of each baculum illustrate a mineralizing proximal region (length = 1). **(C)** Spatial distribution of pores within baculum with the color map represent pore radius from 0 to 20 μm. Big pores such as the medullary canal were not selected for analysis. **(D)** Bar graphs of the average mineral density and porosity of the baculum of each age group illustrate significant differences with age. *$p < 0.05$; **$p < 0.01$; ***$p < 0.001$. P: proximal end. D: distal end.

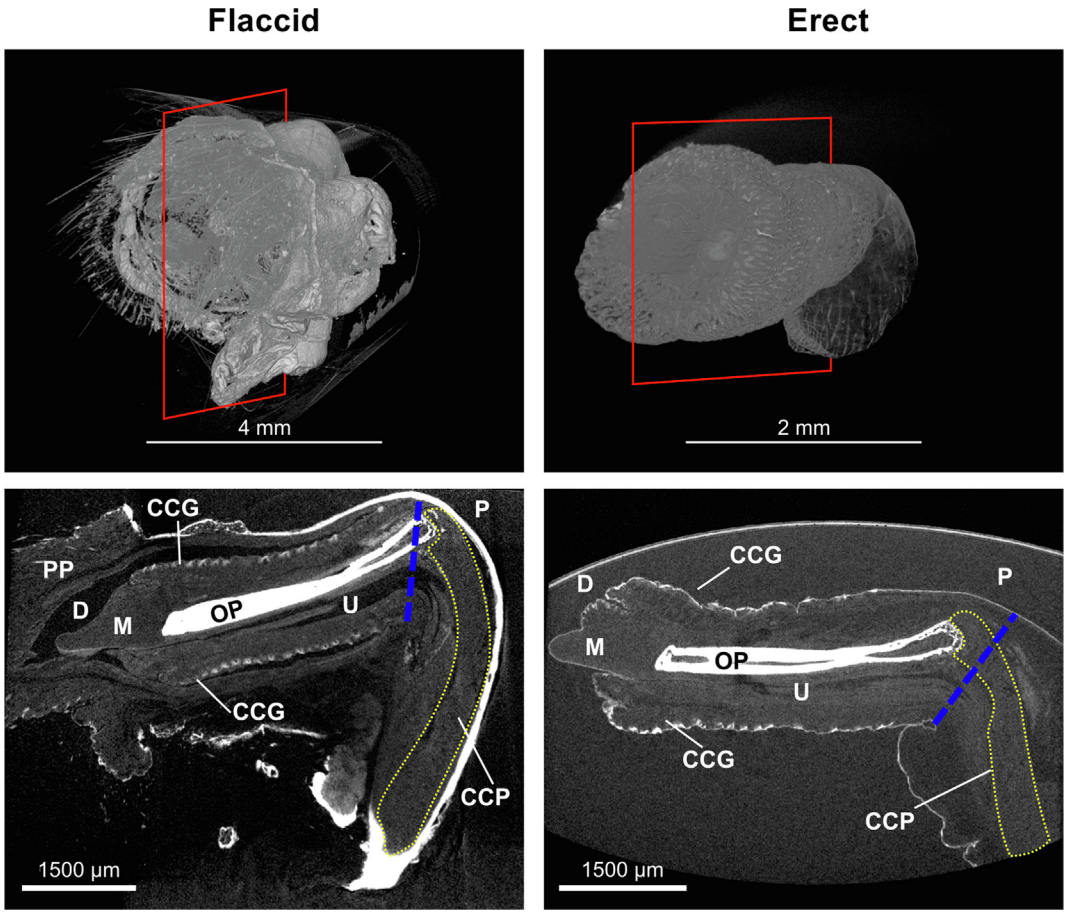


**Fig. 2.** Micro X-ray computed tomography images of a flaccid and an artificially erect penile forms. **Top:** 3D reconstructions illustrate flaccid (left) and erect mouse penile forms (right). The red rectangles indicate the location of subsequent 2D virtual sections (bottom images). **Bottom:** Bottom images are virtual histology sections of the flaccid (left) and erect (right) penile forms. These slices are taken from the middle portion of the baculum as indicated in the above images (red box). The yellow dotted line represents the location of the CCP. The blue line represents the body junction. Please refer to Fig S4 for a better understanding of the 3D spatial arrangement of this organ. P: proximal end. D: distal end. U: urethra. OP: os penis or baculum. M: MUMP. PP: internal and external prepuce. (For interpretation of the references to color in this figure legend, the reader is referred to the web version of this article.)

independent t-tests for collagen CCG and CCP analyses and two-way analysis of variance (ANOVA) with Tukey post-hoc tests for SMC, elastin, and intra-tissue collagen analyses were also performed. All results were considered significant if $p < 0.05$ on a two-tailed significance test.

## 3. Results

### 3.1. Form/shape, mineral density, and porosity of baculum with age

Reconstructed tomographic volumes illustrated a spoon-shaped baculum with a broader proximal (P) and thinner distal (D) region (Fig. 1A). The baculum at the proximal end is an active mineralizing region in younger mice (4–6 week) compared to other regions of the baculum based on mineral density gradients along the length of the baculum (Fig. 1B). The mineral density of the proximal region of a developed baculum (1 year) also was lower in comparison with other regions of the bone, including the central region (Fig. 1B). The mean mineral density of a 1 year old baculum was significantly higher ($p < 0.001$) than baculum from a 6 week old mouse. The internal structures included hollow bony regions with a long medullary canal running through the thin and distal part of the bone. A giant cavity in the proximal region with bony-fingers resembling osteophytes or bony spurs also were observed. The pores within the baculum were primarily situated at the base of the bone and in the distal region, and were comprised of microvasculature (Fig. 1C). A significant correlation between average mineral density with age was observed ($r = 0.908$, $p < 0.001$). Mineral density was significantly different at all ages except for baculum from 5 and 6 week old mice ($p = 0.94$) (Fig. 1D). Porosity was inversely proportional with age ($r = -0.853$, $p < 0.001$) with the porosity in the 1 year old baculum being significantly different from 4, 5, and 6 week old baculum respectively ($p = 0.002$, 0.015, 0.021 respectively) (Fig. 1D).

### 3.2. Penile structures under flaccid and erect forms ex vivo

Micro-XCT scans of the flaccid and erect penile forms illustrated various concentric tubes. The virtual section from the micro-XCT scan of the flaccid penis was at the body-penis junction line (Cunha et al., 2015) (proximal end of the prepucial sheath) (Fig. 2, Fig. S2). The virtual section from the micro-XCT scan of an erect penis illustrated the baculum farther away from the body-penis junction (Fig. 2), and the CCP was longer. The CCP, additionally, was wrapped around the proximal end of the baculum like a sling. The male urogenital mating protuberance (MUMP) ridge, and the space between the CCG and the MUMP, increased as a result of the baculum being pushed further out.

### 3.3. Co-localization of scleraxis and elastin within the CCG and CCP

The CCG from respective 6 week and 1 year old mice was positive for Scx and its presence was not observed in the CCG of 4 and

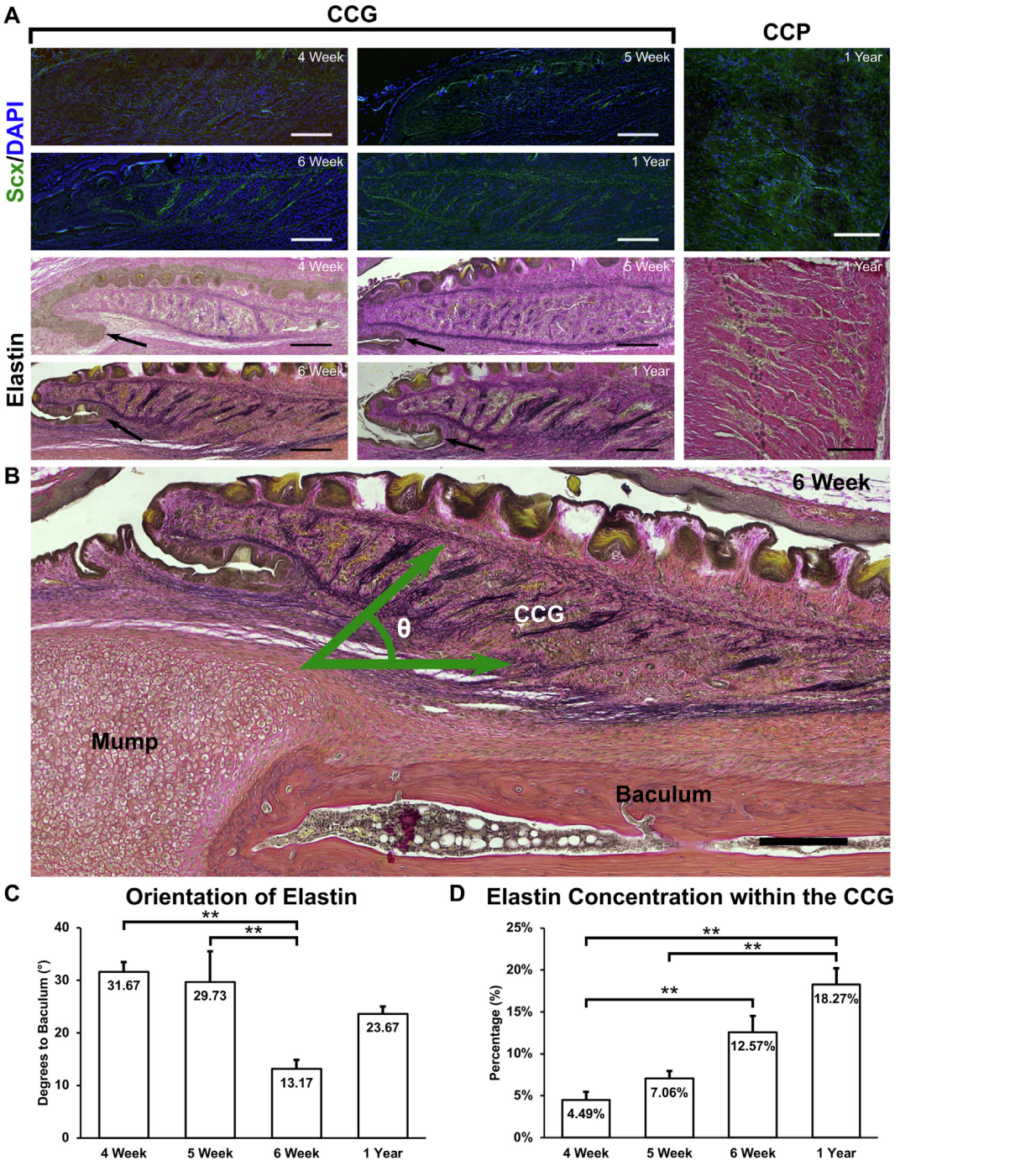


**Fig. 3.** Histomorphometric analyses and mechanoactive regions within a mouse penis. **(A)** Fluorescent and light microscopy images of the corpus cavernosum glandis (CCG) and corpus cavernosum penis (CCP) stained for scleraxis (Scx) and elastin (Verhoeff's Elastin). Scx images were counterstained with DAPI (cell nuclei) and overlaid on brightfield images to illustrate its localization within the tissue. Black arrows point to the developing MUMP ridge of the mouse penis. **(B)** Higher magnification image illustrates the relationship between elastin fibers in the CCG with the baculum and MUMP. The green arrows and $\theta$ represent the orientation of elastin fibers calculated in **(C)**. All scale bars represent 200 μm. **(C)** Average orientation of the elastin fibers relative to the baculum with age are shown. An angle of 0° would indicate that the elastin fibers were parallel to the baculum. **(D)** Elastin content, represented as a percentage of the whole tissue, within the CCG with age are shown. No significant expression of elastin within the CCP. $^{**}p < 0.01$. $^{***}p < 0.001$ was observed. (For interpretation of the references to color in this figure legend, the reader is referred to the web version of this article.)

5 week old mice (Fig. 3A). The CCP also contained Scx, but it was localized to the edges of the tissue and was not orientation specific (Fig. 3A). The CCG also contained an abundance of elastin that was orientated at an angle of 18 ± 2° relative to the baculum in developing and functionally active mice (6 week) and this orientation was also observed at 1 year of age (Fig. 3C). Elastin was also present within the CCG of younger mice with a higher average orientation over a wider range (larger standard deviation) (Fig. 3C) and was heavily localized along collagenous struts and the collagenous outer layer of the CCG (Figs. 3A and 4A). A moderate correlation of elastin with collagen contents was observed with age ($r = 0.62$; $p < 0.0001$) (Fig. 3D). Elastin was limitedly expressed in the CCP. There was also a noticeable difference in the structure of the MUMP ridge as the penis developed (Fig. 3A). The ridge appeared open and a gap was visualized as an increased surface area between the CCG and the MUMP appeared.

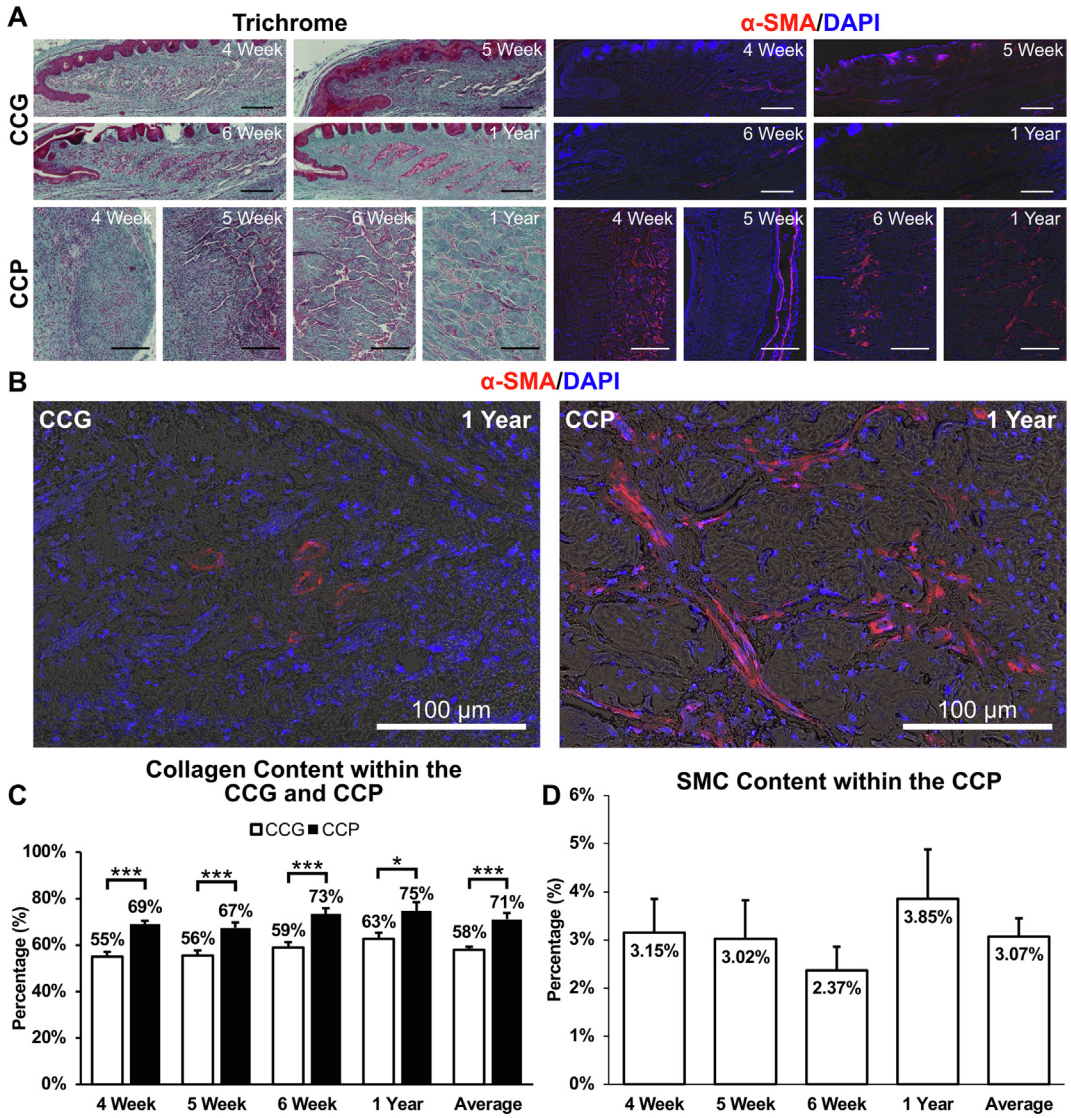


**Fig. 4.** Collagen and smooth muscle cell (SMC) concentration within the corpus cavernosum glandis (CCG) and corpus cavernosum penis (CCP). **(A)** Fluorescence and light microscopy images of CCG and CCP stained for collagen (Masson's trichrome) and α-smooth muscle actin (α-SMA) with age are shown. α-SMA sections were also stained with DAPI (cell nuclei) and were correlated with structure by overlaying with bright field images. Scale bars represent 200 μm. **(B)** Higher magnification images of the CCG and CCP of a 1 year old mouse penis stained for α-SMA (red fluorescent). The sections were counterstained with DAPI (cell nuclei) and were overlaid with bright field images. **(C)** Percentage of collagen variation within the CCG and CCP as well as overall average, and **(D)** percentage of α-SMA within the CCP with the overall mouse average with age are shown. No significant expression of α-SMA was observed for the CCG. *$p < 0.05$; ***$p < 0.001$. (For interpretation of the references to color in this figure legend, the reader is referred to the web version of this article.)

### *3.4. Spatial localization of collagen, smooth muscle, and nerves within a mouse penis*

The Scx positive collagen within the CCG appeared primarily in oblique struts. Collagen also lined the external aspect of the CCG. The CCP also contained a significant amount of wavy collagen that resembled the structure of an accordion. Collagen occupied area within the CCG was statistically less than that observed in the CCP for any given age ($p < 0.05$) (Fig. 4C). The CCG collagen content was positively correlated with age ($r = 0.33$, $p = 0.0203$), whereas the CCP was not ($p > 0.05$). Bundles of collagen in the CCP formed into rows as the penis developed (Fig. 4A).

Immunolocalization of biomolecules indicated limited amounts of α-SMA(+) SMC in CCG with age albeit its existence within blood vessels (Fig. 4). Quantifiable amount of α-SMA(+) SMCs with an overall average of 3 ± 0.4% was observed in the CCP (Fig. 4D). No correlation between α-SMA(+) SMC with age was observed ($p > 0.05$); however, α-SMA(+) SMCs within the CCP were dispersed throughout collagen and were associated with sinusoidal space (Fig. 4B). Field emission – scanning electron microscopy of a 6 week old mouse penis revealed erythrocytes within the CCG and CCP (Fig. 5A). Immunolocalization of PGP 9.5 revealed nerves within the CCG and CCP, and in the outer layer of the CCG (black arrows in Fig. 5C). The nerves on the outside of the CCG wrapped around the entire erectile tissue in multiple bundles. The cavernosum nerve was also identified on the outside of the CCP (red arrow in Fig. 5C).

## 4. Discussion

The overall objective of this study was to map in space and time the structure and biochemical composition of various tissues within the penis of a mouse, and thereby postulate biomechanically active sites within a penis of a Scx-GFP transgenic mouse model. Spatio-temporal maps using various imaging modalities

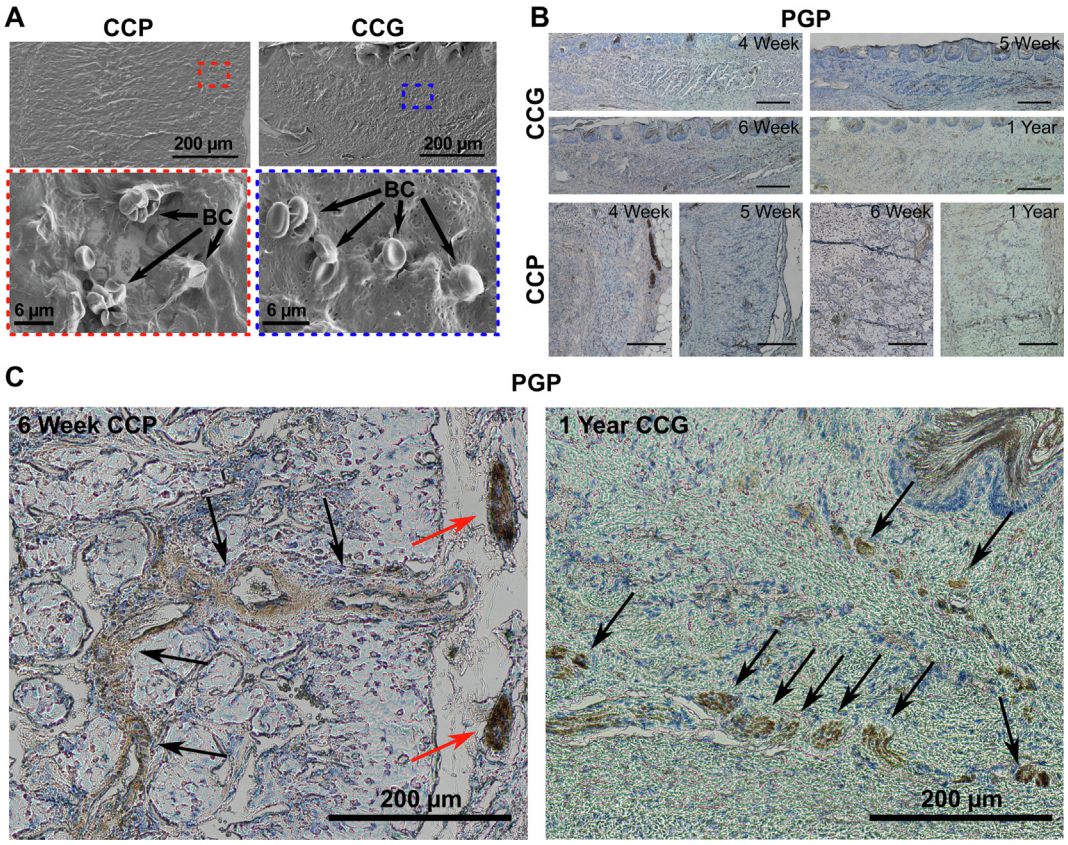


**Fig. 5.** Nerve and erythrocyte distribution within the corpus cavernosum glandis (CCG) and corpus cavernosum penis (CCP). **(A)** Field emission – scanning electron microscopy images of a 6 week mouse penis CCG and the CCP illustrated erythrocytes within the tissue. Colored boxes indicate the location of higher magnification images in the bottom row. BC: red blood cell. **(B)** Light microscopy images of the CCG and CCP stained for protein gene product 9.5 (PGP) with age are shown. Scale bars represent 200 μm. **(C)** Higher magnification of a 6 week old CCP (left) and 1 year old CCG (right) and mouse penile tissue stained for PGP. Black arrows indicate location of nerves and the red arrow denotes the cavernosal nerve. Scale bars represent 200 μm. (For interpretation of the references to color in this figure legend, the reader is referred to the web version of this article.)

illustrated that (a) the baculum continues to grow in length past pre-pubescent age of a mouse; (b) the CCG is equivalent to the corpus cavernosum (CC) in humans and common denominators include SMCs, nerves, collagen, and elastin; and (c) correlate the above two objectives to highlight the relevance of structure and function of CCG, CCP, and baculum toward overall functional biomechanics of a mouse penis.

### *4.1. The bony-baculum continues to grow in length past pre-pubescent age of a mouse*

Male mice typically reach sexual maturity at 6–8 weeks, and begin breeding around 6 weeks of age (Engle and Rosasco, 1927; Kirkham, 1920). This means that the penis is functional at 6 weeks; however, the baculum is not fully grown and ossified as is observed by lower mineral density at the proximal end (Fig. 1). Endochondral bone growth at the proximal end of the baculum (Murakami, 1986; Murakami and Mizuno, 1984) continues past the age of sexual maturity as denoted by the higher porosity and lower mineral density (Fig. 1D) of the 6 week mouse baculum. When comparing the morphological details of baculum from 6 week and 1 year mice respectively, a noticeable size difference in relation to the length (Fig. 1) of the baculum, but proportional to size of the mammal was observed.

Baculum continues to grow with age (Fig. 1). Similar to skeletal bone in most mammals, the developmental and functional elongation of the baculum occurs at the growth plate which is located at the proximal end of the baculum and was observed in rats (Vilmann and Vilmann, 1983). In comparison to the mineral densities of cortical and trabecular bone of mouse and rat femurs at 9 and 20 weeks of age, the baculum's mineral density at 5 weeks and older (Fig. 1D) was significantly greater (Oftadeh et al., 2015; Verdelis et al., 2008). The mouse baculum has a similar mineral density to that of the human alveolar bone, and this result contradicts previous thoughts that the baculum was lower in mineral density as compared to load-bearing organs (Sharir et al., 2011). While the baculum is typically non-load bearing, during copulation, it does bear a certain load via pressures from within the penis as well as vaginal pressure. In analyzing the mineral density along the normalized length, the highest mineral density was at the distal to the center of the baculum; the region farthest from the CCP (Fig. 1B, Fig. S2).

### *4.2. The CCG is equivalent to CC in humans and common denominators include SMCs, nerves, collagen, and elastin*

Rodents are often used as models to study the mechanisms of various penile pathologies such as erectile dysfunction and Peyronie's disease. Often, pathologies are dependent on the stiffness of the ECM, cell differentiation, cell arrangement, and biomolecular localization within tissues; thus, they can promote changes in local tissue mechanics that permit overall penile biomechanics and function. For this reason, it is important to note the relative expressions of proteins that contribute to the biomechanics of the ECM (elastin, collagen, and functional aspects of SMCs with nerves) in

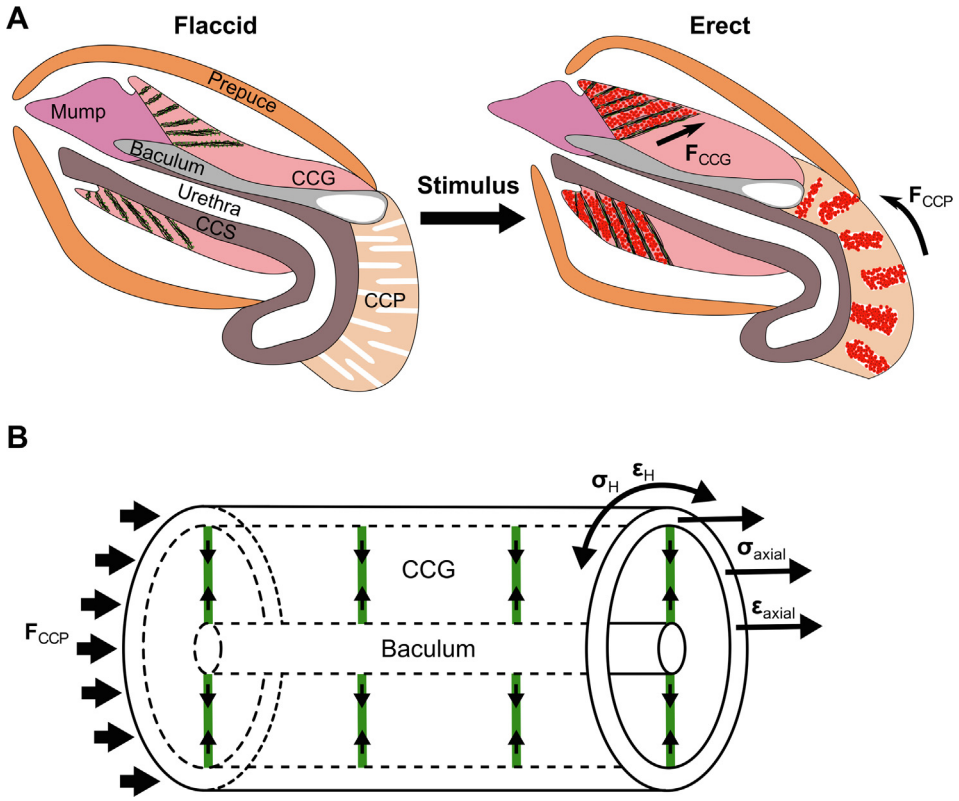


**Fig. 6.** Schematic of biomechanical forces acting within the mouse penis during an erection and how it influences the adjacent tissues. **(A)** A general schematic represents flaccid (left) and erect penile forms (right). Arrows indicate the direction of the forces. The red dots in the erect state represent blood. $\mathbf{F}_{CCG}$ is the force from the corpus cavernosum glandis (CCG) pressure. $\mathbf{F}_{CCP}$ is the force from the pressure within the corpus cavernosum penis (CCP). **(B)** Cylindrical piston schematic illustrating the stress and strain on the CCG due to the internal hemodynamic pressure. $\boldsymbol{\sigma}_H$ and $\epsilon_H$ represent the hoop stress and strain respectively and $\boldsymbol{\sigma}_{axial}$ and $\boldsymbol{\epsilon}_{axial}$ represent the axial stress and strain. The green lines indicate collagenous struts that counteract the hoop stress. The $\mathbf{F}_{CCP}$ acts on the proximal end of the cylinder resulting in horizontal displacement for both bodies. CCS: corpus cavernosum spongiosum. (For interpretation of the references to color in this figure legend, the reader is referred to the web version of this article.)

a mouse and how the expressions of the biomolecules change with age.

The CCP in mice has been used to model Peyronie's disease and erectile dysfunction as it is the anatomically equivalent tissue to the human CC; however, our results illustrated large differences in collagen and SMC contents within the CCP and CCG in a mouse. These results concur with studies by others, in that, the human CC contains a lower percentage of collagen and a higher percentage of SMC as compared to the mouse and rat CCPs respectively (Piao et al., 2007; Pinheiro et al., 2000). Our study showed that the CCG has a lower collagen content (58 ± 1%) and was consistently significantly lower than that observed in the CCP. The CCG resides within the glans of the mouse penis, which is external to the body and is a circular body of erectile tissue that surrounds the urethra, baculum, and corpus cavernosum spongiosum (Phillips et al., 2015) (Fig. S4). Furthermore, the CCG contains trabeculae that are coated with elastin (Fig. 3A), similar to the collagenous struts in the human CC and shows an increase in collagen with age ($r = 0.33$; $p = 0.02$) (Brock et al., 1997; Ferrer et al., 2010). The CCG also contained SMCs around blood vessels; however, there was not enough tissue to quantify the amount of SMCs within the CCG because these biochemical assays were performed under flaccid conditions and at different sectioning angles.

Blood vessels containing erythrocytes visualized using FE-SEM and immunolocalized nerves were found between the collagenous struts (Fig. 5A) indicating that this tissue is filled with blood during normal function, as would be expected in an erectile tissue. Nerve bundles were identified on the proximal end of the CCG in the collagenous outer layer localized near the SMC in blood vessels. The stimulation of the cavernosal nerve (red arrows in Fig. 5C) within the CCP causes the SMC within the CCP to relax and prompts an erection of the penis in a rodent (Piao et al., 2007); however, it is unknown if this nerve connects directly to the bundle of nerves in the CCG. The function of a few nerves observed in the distal, collagenous outer layer of the CCG is yet to be determined.

### *4.3. Structure and function of CCG, CCP, and baculum toward the overall biomechanics of a mouse penis*

Scx is a basic helix-loop-helix transcription factor that is expressed in tendon and ligament cells and is a strong transactivator (Cserjesi et al., 1995; Espira et al., 2009). Scx is a mechanosensitive marker for tendons, ligaments, and other developing connective tissues in musculoskeletal system that are continuously subjected to forces as they grow and/or when in function (Schweitzer et al., 2001).

Scx is expressed in the collagenous struts of the CCG indicating their mechanosensitivity likely during native erection (relative to sexually active mice). The 4 and 5 week old mice penises didn't express Scx due to the lack of native erections. In rats, copulatory ability is acquired between 45 and 75 days which corresponds to roughly 6 week, and rat erections can be induced via volatile odors from nearby female rats (Hull and Dominguez, 2007; Plant et al., 2016). Additionally, elastin is an important ECM fibrillar protein that readily deforms and facilitates structural changes to meet functional demands. As such, it is conceivable that a change in elastin content and associated matrix protein expressions could lead to changes in mechanical integrity of respective tissues. Therefore, resulting hemodynamic pressure increase during a native erection will cause circumferential strain ($\epsilon_H$) (the shape of a penis can be

approximated to be a cylinder) which must be balanced by elastin-rich collagenous struts (Fig. 6B). Further, if the baculum and MUMP "jet" out from a capsule (the glans), as it is pushed by the expanding CCP (Fig. 2), the angle of the elastin fibers ($\theta$) relative to baculum could change. Additionally, the increase in elastin with age (Fig. 3D) could be indicative of increased function and/or age. Previous studies have identified that the mouse CCP expands and maintains a higher pressure due to increased blood flow (Mizusawa et al., 2001; Piao et al., 2007; Sezen and Burnett, 2000) indicating the need for collagen interspersed with elastin.

The radially arranged collagenous struts within the CCG may act as support beams specifically when in function (Brock et al., 1997). Similarly, the CCP also fills with blood and maintains a high internal pressure so as to push the glans of the penis further out thereby straightening the penis resulting from pressure on the proximal end of the baculum. Based on this proof-of-concept study, the CCG serves as the primary erectile tissue that keeps the penis stiff following blood flow. However, *in silico* simulations studies are warranted to specifically highlight the effect of the observed overall form including the internal architecture on penile function.

## Acknowledgements

The authors would like to thank Ms. Grace Nonomura for her help in specimen preparation and Ms. Linda Prentice for assistance with histology. The authors thank the Biomaterials and Bioengineering Correlative Microscopy Core (http://bbcmc.ucsf.edu), UCSF for the use of their MicroXCT-200 and SIGMA 500-VP Field Emission Electron Microscope – Scanning and Transmission. This work was supported by the National institutes of Health [R21 DK109912 (SPH,MLS); R01 DE022032 (SPH)].

## Declaration of Competing Interest

The authors declare they have no conflict of interest.

## Author contributions

S.P.H. conceived the study; S.P.H. and M.S. provided funding; M. R.H., S.P.H., L.C. further designed the study; S.P.H. provided the specimens; L.C., B.W., and M.R.H. performed the dissections; L.C., M.R.H., and M.K. assisted in data collection; M.R.H. and S.P.H analysed the data and wrote the manuscript; all authors reviewed and approved the article.

## Appendix A. Supplementary material

Supplementary data to this article can be found online at https://doi.org/10.1016/j.jbiomech.2020.109637.

## References

Ankel-Simons, F., 2007. Primate Anatomy, Primate Anatomy. Elsevier. doi: 10.1016/B978-0-12-372576-9.X5000-1.

Auguie, B., 2016. gridExtra: Miscellaneous Functions for "Grid" Graphics.

Beckett, S.D., Hudson, R.S., Walker, D.F., Vachon, R.I., Reynolds, T.M., 1972. Corpus cavernosum penis pressure and external penile muscle activity during erection in the goat. Biol. Reprod. 7, 359–364.

Beckett, S.D., Walker, D.F., Hudson, R.S., Reynolds, T.M., Vachon, R.I., 1974. Corpus cavernosum penis pressure and penile muscle activity in the bull during coitus. Am. J. Vet. Res. 35, 761–764.

Bivalacqua, T.J., Diner, E.K., Novak, T.E., Vohra, Y., Sikka, S.C., Champion, H.C., Kadowitz, P.J., Hellstrom, W.J., 2000. A rat model of Peyronie's disease associated with a decrease in erectile activity and an increase in inducible nitric oxide synthase protein expression. J. Urol. 163, 1992–1998.

Brindle, M., Opie, C., 2016. Postcopulatory sexual selection influences baculum evolution in primates and carnivores. Proc. R. Soc. B Biol. Sci. 283, 20161736. https://doi.org/10.1098/rspb.2016.1736.

Brock, G., Hsu, G.L., Nunes, L., von Heyden, B., Lue, T.F., 1997. The anatomy of the tunica albuginea in the normal penis and Peyronie's disease. J. Urol. 157, 276–281. https://doi.org/10.1097/00005392-199701000-00096.

Burt, W.H., 1936. A study of the baculum in the genera Perognathus and Dipodomys. J. Mammal. 17, 145–156. https://doi.org/10.2307/1374190.

Cserjesi, P., Brown, D., Ligon, K.L., Lyons, G.E., Copeland, N.G., Gilbert, D.J., Jenkins, N. A., Olson, E.N., 1995. Scleraxis: a basic helix-loop-helix protein that prefigures skeletal formation during mouse embryogenesis. Development 121, 1099–1110.

Cunha, G.R., Sinclair, A., Risbridger, G., Hutson, J., Baskin, L.S., 2015. Current understanding of hypospadias: relevance of animal models. Rev. Urol. Nat. https://doi.org/10.1038/nrurol.2015.57.

Davila, H.H., Ferrini, M.G., Rajfer, J., Gonzalez-Cadavid, N.F., 2003. Fibrin as an inducer of fibrosis in the tunica albuginea of the rat: a new animal model of Peyronie's disease. BJU Int. 91, 830–838.

Dean, R.C., Lue, T.F., 2005. Physiology of penile erection and pathophysiology of erectile dysfunction. Urol. Clin. North Am. 32, 379–395. https://doi.org/10.1016/j.ucl.2005.08.007.

Djomehri, S.I., Candell, S., Case, T., Browning, A., Marshall, G.W., Yun, W., Lau, S.H., Webb, S., Ho, S.P., 2015. Mineral density volume gradients in normal and diseased human tissues. PLoS ONE 10, 1–24. https://doi.org/10.1371/journal.pone.0121611.

El-Sakka, A.I., Hassoba, H.M., Chui, R.M., Bhatnagar, R.S., Dahiya, R., Lue, T.F., 1997. An animal model of Peyronie's-like condition associated with an increase of transforming growth factor beta mRNA and protein expression. J. Urol. 158, 2284–2290. https://doi.org/10.1016/S0022-5347(01)68236-3.

Engle, E.T., Rosasco, J., 1927. The age of the albino mouse at normal sexual maturity. Anat. Rec. 36, 383–388. https://doi.org/10.1002/ar.1090360410.

Espira, L., Lamoureux, L., Jones, S.C., Gerard, R.D., Dixon, I.M.C., Czubryt, M.P., 2009. The basic helix-loop-helix transcription factor scleraxis regulates fibroblast collagen synthesis. J. Mol. Cell. Cardiol. 47, 188–195. https://doi.org/10.1016/j.yjmcc.2009.03.024.

Ferrer, J.E., Velez, J.D., Herrera, A.M., 2010. Age-related morphological changes in smooth muscle and collagen content in human corpus cavernosum. J. Sex. Med. 7, 2723–2728. https://doi.org/10.1111/j.1743-6109.2009.01508.x.

Ferretti, L., Fandel, T.M., Qiu, X., Zhang, H., Orabi, H., Wu, A.K., Banie, L., Wang, G., Lin, G., Lin, C.-S., Lue, T.F., 2014. Tunica albuginea allograft: a new model of LaPeyronie's disease with penile curvature and subtunical ossification. Asian J. Androl. 16, 592–596. https://doi.org/10.4103/1008-682X.125900.

Fonck, E., Feigl, G.G., Fasel, J., Sage, D., Unser, M., Rüfenacht, D.A., Stergiopulos, N., 2009. Effect of aging on elastin functionality in human cerebral arteries. Stroke 40, 2552–2556. https://doi.org/10.1161/STROKEAHA.108.528091.

Gilbert, S.F., Zevit, Z., 2001. Congenital human baculum deficiency: the generative bone of genesis 2:21–23 [2]. Am. J. Med. Genet. 101, 284–285. https://doi.org/10.1002/ajmg.1387.

Hanyu, S., Iwanaga, T., Kano, K., Sato, S., 1987. Mechanism of penile erection in the dog. Pressure-flow study combined with morphological observation of vascular casts. Urol. Int. 42, 401–412.

Harrel Jr., F.E., Dupont, C., 2017. Hmisc: Harrell Miscellaneous.

Herdina, A.N., Herzig-Straschil, B., Hilgers, H., Metscher, B.D., Plenk, H., 2010. Histomorphology of the penis bone (baculum) in the gray long-eared bat Plecotus austriacus (Chiroptera, Vespertilionidae). Anat. Rec. 293, 1248–1258. https://doi.org/10.1002/ar.21148.

Hull, E.M., Dominguez, J.M., 2007. Sexual behavior in male rodents. Horm. Behav. 52, 45–55. https://doi.org/10.1016/j.yhbeh.2007.03.030.

Kelly, D.A., 2000. Anatomy of the baculum-corpus cavernosum interface in the Norway rat (Rattus norvegicus), and implications for force transfer during copulation. J. Morphol. 244, 69–77. https://doi.org/10.1002/(SICI)1097-4687(200004)244:1<69::AID-JMOR7>3.0.CO;2-#.

Kifor, I., Williams, G.H., Vickers, M.A., Sullivan, M.P., Jodbert, P., Dluhy, R.G., 1997. Tissue angiotensin II as a modulator of erectile function. I. Angiotensin peptide content, secretion and effects in the corpus cavernosum. J. Urol. 157, 1920–1925.

Kirkham, W.B., 1920. The life of the white mouse. Exp. Biol. Med. 17, 196–198. https://doi.org/10.3181/00379727-17-104.

Lee, J.-H., Pryce, B.A., Schweitzer, R., Ryder, M.I., Ho, S.P., 2015. Differentiating zones at periodontal ligament-bone and periodontal ligament-cementum entheses. J. Periodontal Res. 50, 870–880. https://doi.org/10.1111/jre.12281.

Lucattelli, M., Lunghi, B., Fineschi, S., Mirone, V., di Villa Bianca, R. d'Emmanuele, Longo, N., Imbimbo, C., De Palma, R., Sorrentino, R., Lungarella, G., Cirino, G., 2008. A new mouse model of Peyronie's disease: An increased expression of hypoxia-inducible factor-1 target genes during the development of penile changes. Int. J. Biochem. Cell Biol. 40, 2638–2648. doi: 10.1016/j.biocel.2008.05.012.

Martínez-Piñeiro, L., Brock, G., Trigo-Rocha, F., Hsu, G.L., Lue, T.F., Tanagho, E.A., 1994. Rat model for the study of penile erection: pharmacologic and electrical-stimulation parameters. Eur. Urol. 25, 62–70.

Mizusawa, H., Hedlund, P., Håkansson, A., Alm, P., Andersson, K.E., 2001. Morphological and functional in vitro and in vivo characterization of the mouse corpus cavernosum. Br. J. Pharmacol. 132, 1333–1341. https://doi.org/10.1038/sj.bjp.0703938.

Murakami, R., 1986. Development of the os penis in genital tubercles cultured beneath the renal capsule of adult rats. J. Anat. 149, 11–20.

Murakami, R., Mizuno, T., 1984. Histogenesis of the Os Penis and Os Clitoridis in Rats. (chondrogenesis/bone formation/testosterone/genital tubercle). Dev. Growth Differ. 26, 419–426. https://doi.org/10.1111/j.1440-169X.1984.00419.x.

Nieminen, H.J., Ylitalo, T., Karhula, S., Suuronen, J.-P., Kauppinen, S., Serimaa, R., Hæggström, E., Pritzker, K.P.H., Valkealahti, M., Lehenkari, P., Finnilä, M., Saarakkala, S., 2015. Determining collagen distribution in articular cartilage using contrast-enhanced micro-computed tomography. Osteoarthr. Cartil. 23, 1613–1621. https://doi.org/10.1016/j.joca.2015.05.004.

Oftadeh, R., Entezari, V., Spörri, G., Villa-Camacho, J.C., Krigbaum, H., Strawich, E., Graham, L., Rey, C., Chiu, H., Müller, R., Hashemi, H.N., Vaziri, A., Nazarian, A., 2015. Hierarchical analysis and multi-scale modelling of rat cortical and trabecular bone. J. R. Soc. Interface 12. https://doi.org/10.1098/rsif.2015.0070.

Penson, D.F., Ng, C., Rajfer, J., Gonzalez-Cadavid, N.F., 1997. Adrenal control of erectile function and nitric oxide synthase in the rat penis. Endocrinology 138, 3925–3932. https://doi.org/10.1210/endo.138.9.5402.

Phillips, T.R., Wright, D.K., Gradie, P.E., Johnston, L.A., Pask, A.J., 2015. A comprehensive atlas of the adult mouse penis. Sex. Dev. 9, 162–172. https://doi.org/10.1159/000431010.

Piao, S., Ryu, J.K., Shin, H.Y., Han, J.Y., Lee, H.S., Suh, J.K., 2007. The mouse as a model for the study of penile erection: moving towards a smaller animal. Int. J. Androl. 30, 452–457. https://doi.org/10.1111/j.1365-2605.2006.00737.x.

Pinheiro, A.C., Costa, W.S., Cardoso, L.E., Sampaio, F.J., 2000. Organization and relative content of smooth muscle cells, collagen and elastic fibers in the corpus cavernosum of rat penis. J. Urol. 164, 1802–1806. https://doi.org/10.1016/S0022-5347(05)67110-8.

Plant, T.M. (Tony M.., Zeleznik, A., Knobil, E., 2016. Knobil and Neill's Physiology of Reproduction, Knobil and Neill's Physiology of Reproduction. doi: 10.1016/c2011-1-07288-0.

Pryce, B.A., Brent, A.E., Murchison, N.D., Tabin, C.J., Schweitzer, R., 2007. Generation of transgenic tendon reporters, ScxGFP and ScxAP, using regulatory elements of the scleraxis gene. Dev. Dyn. 236, 1677–1682. https://doi.org/10.1002/dvdy.21179.

Püspöki, Z., Storath, M., Sage, D., Unser, M., 2016. Transforms and operators for directional bioimage analysis: a survey. Adv. Anat. Embryol. Cell Biol. 219, 69–93. https://doi.org/10.1007/978-3-319-28549-8_3.

R Core Team, 2017. R: A language and environment for statistical computing.

Schultz, N.G., Lough-Stevens, M., Abreu, E., Orr, T., Dean, M.D., 2016. The Baculum was Gained and Lost Multiple Times during Mammalian Evolution. In: Integrative and Comparative Biology. Oxford University Press, pp. 644–656. doi: 10.1093/icb/icw034.

Schweitzer, R., Chyung, J.H., Murtaugh, L.C., Brent, E., Rosen, V., Olson, E.N., Lassar, A., Tabin, C.J., 2001. Analysis of the tendon cell fate using Scleraxis, a specific marker for tendons and ligaments. Development 128, 3855–3866.

Scott, A., Danielson, P., Abraham, T., Fong, G., Sampaio, A.V., Underhill, T.M., 2011. Mechanical force modulates scleraxis expression in bioartificial tendons. J. Musculoskelet. Neuronal Interact. 11, 124–132.

Sezen, S.F., Burnett, A.L., 2000. Intracavernosal pressure monitoring in mice: responses to electrical stimulation of the cavernous nerve and to intracavernosal drug administration. J. Androl. 21, 311–315.

Sharir, A., Israeli, D., Milgram, J., Currey, J.D., Monsonego-Ornan, E., Shahar, R., 2011. The canine baculum: the structure and mechanical properties of an unusual bone. J. Struct. Biol. 175, 451–456. https://doi.org/10.1016/j.jsb.2011.06.006.

Stockley, P., Ramm, S.A., Sherborne, A.L., Thom, M.D.F., Paterson, S., Hurst, J.L., 2013. Baculum morphology predicts reproductive success of male house mice under sexual selection. BMC Biol. 11, 66. https://doi.org/10.1186/1741-7007-11-66.

Sugimoto, Y., Takimoto, A., Hiraki, Y., Shukunami, C., 2013. Generation and characterization of ScxCre transgenic mice. Genesis 51, 275–283. https://doi.org/10.1002/dvg.22372.

Verdelis, K., Ling, Y., Sreenath, T., Haruyama, N., MacDougall, M., van der Meulen, M. C.H., Lukashova, L., Spevak, L., Kulkarni, A.B., Boskey, A.L., 2008. DSPP effects on in vivo bone mineralization. Bone 43, 983–990. https://doi.org/10.1016/j.bone.2008.08.110.

Vilmann, A., Vilmann, H., 1983. Os penis of the rat. IV. The proximal growth cartilage. Acta Anat. (Basel) 117, 136–144. https://doi.org/10.1128/AAC.03728-14.

Wickham, H., 2016. gtable: Arrange "Grobs" in Tables.

Yilmaz, I.E., Barazani, Y., Tareen, B., 2013. Penile ossification: a traumatic event or evolutionary throwback? Case report and review of the literature. J. Can. Urol. Assoc. 7, 112–114. https://doi.org/10.5489/cuaj.249.